Available online at www.sciencedirect.com
ScienceDirect
Trans. Nonferrous Met. Soc. China 30(2020) 363−372
Transactions of Nonferrous Metals Society of China
www.tnmsc.cn

Mechanical properties and corrosion behaviors of Mg−4Zn−0.2Mn−0.2Ca alloy after long term in vitro degradation

Yuan-fen CHENG, Wen-bo DU, Ke LIU, Jun-jian FU, Zhao-hui WANG, Shu-bo LI, Jin-long FU

College of Materials Science and Engineering, Beijing University of Technology, Beijing 100124, China

Received 22 April 2019; accepted 6 December 2019

Abstract: An extruded Mg−4Zn−0.2Mn−0.2Ca alloy was developed as potential biodegradable bone-plate due to its excellent biocompatibility. Long term in vitro immersion in Hank's solution and bending test were used to evaluate the degradability and the mechanical integrity of the alloy. The results revealed that the degradation rate of the bone-plate increased in the first 7 days and then decreased with the prolonged immersion time before it finally reached a steady stage (about 0.84 mm/a) after immersion for 90 days. The bending strength after immersion for 60 days was 67.6 MPa, indicating that the bone-plate could support certain mechanical load after long term degradation. The formation of corrosion pits after degradation stemmed from the separation of the continuously distributed second phases from Mg matrix under the action of micro-galvanic couples. As a result, the mechanical performance of Mg−4Zn−0.2Mn−0.2Ca alloy was aggravated owing to the corrosion holes on its surface.

Key words: magnesium alloys; bending strength; corrosion behaviors; in vitro degradation; bone-plate

1 Introduction

At present, stainless steel, titanium and cobalt−chromium alloys have been widely used as implants in clinical medicine. However, a number of drawbacks exist when these alloys are applied as implant materials. Firstly, they are lack of biological activity. The metal ions or particles will fall into human bodies because of wear or corrosion during implantation, easily causing local allergic reactions and inflammation [1]. Secondly, they are non-degradable and need to be taken out by the second surgery after human bones healing, thus, not only increasing the pain of patients, but also increasing the cost of treatment and the risk of medicine [2]. Thirdly, they do not match with human bone tissues due to their high elastic modulus. Therefore, it is of great significance to develop a new kind of biodegradable alloy, which can exhibit favorable biocompatibility as well as mechanical compatibility to human bones.

Magnesium (Mg) alloys have been hailed as the third generation biomedical materials because of their unique physical and biological properties [3,4]. For example, their density and elastic modulus are close to those of human natural bones, and their higher specific strength and stiffness can provide stable mechanical support in the initial period of implantation [5,6]. In addition, the mechanical properties of Mg alloys decrease slowly rather than abruptly during human bones regeneration, which is beneficial to alleviating the effect of stress shielding and avoiding the slow healing. However, the clinical applications of Mg alloys are still seriously hampered due to the rapid corrosion rate. Although

Foundation item: Projects (2016YFB0301001, 2016YFB0301101) supported by the National Key Research and Development Program of China; Project (51801004) supported by the National Natural Science Foundation of China; Project (KM201710005005) supported by Beijing Municipal Education Commission, China; Projects (2172013, 2192006) supported by Beijing Natural Science Foundation, China

Corresponding author: Wen-bo DU; Tel/Fax: +86-10-67392917; E-mail: duwb@bjut.edu.cn

DOI: 10.1016/S1003-6326(20)65218-9

some researchers [7−9] have proved that Mg alloys containing rare earth elements or aluminum element had comparatively good corrosion resistance and considerable tensile strength, unfortunately, these alloys are not yet suitable for biomedical applications. It is reported that aluminum and rare earth elements may cause neurotoxicity, which raises the risk of cell proliferation thrombosis [10,11]. Even though an idea is that human body can accept a low content of aluminum or rare earth elements, the corresponding detailed research is still needed to prove their biosafety [12].

Usually, elements such as Zn, Mn and Ca are selected to develop the biodegradable Mg alloys, because they are not only nontoxic but also beneficial to improving the performance of Mg alloys [13−15]. As reported, Ca was able to enhance the formation of new bones and accelerate the rate of bone growth [16], Mn could significantly refine the microstructure and improve the corrosion performance of Mg alloys [17]. XU et al [18,19] carried out the corrosion test of Mg−Mn−Zn alloy in vitro and in vivo. Their results showed that 54% of the alloy degraded on the 14th day, and Zn and Mn elements uniformly distributed in implants after 18 weeks' post-operation. The corrosion layers and the surrounding bone tissues indicated that Zn and Mn elements were easily absorbed by bio-environment.

It is essential for any temporary implant to have sufficient strength for maintaining its mechanical integrity under the synergistic action of human mechanical loading characteristic and corrosion physiology environment [20]. As the basic mechanical requirement of magnesium alloy for bone implantation, the yield strength is not less than 200 MPa and the elongation rate is more than 15% at room temperature [21]. The fixation of fractured bones takes at least 3 months until complete healing [22]. This means that Mg alloys, as temporary orthopedic fixtures, have to hold sufficient strength until 3 months' degradation. However, the previous works seldom focused on the degradation of Mg alloys in vitro immersion for more than 1 month [23−26]. BOWEN et al [23] immersed pure Mg filaments in cell culture media up to 16 days, and found that the tensile strength of the samples decreased linearly from 240 to 150 MPa on the 13th day and spontaneously destroyed on the 14th day. HE et al [24] investigated the in vitro degradation of an extruded Mg−6Zn−Mn alloy, and found that its corrosion rate was (1.01±0.10) mm/a after immersion for 1 month. DU et al [26] developed a kind of Mg−Zn−Mn−Ca alloy, and studied the mechanical properties and corrosion behaviors of the as-cast Mg−4Zn−0.2Mn−0.2Ca alloy, but the degradation experiment was only limited to 40 days. Nevertheless, there remains a lack of data that assess long term in vitro degradation of Mg alloys. In the present study, we focus on the mechanical properties as well as the degradation behaviors of an extruded Mg−4Zn−0.2Mn−0.2Ca alloy after long term in vitro immersion. Also, the bone plates made of the alloy are detected based on the alloy investigation.

2 Experimental

2.1 Raw materials and methods

The ingot of Mg−4Zn−0.2Mn−0.2Ca alloy was prepared by melting pure Mg (99.99 wt.%), pure Zn (99.99 wt.%), Mg−9.4wt.%Ca and Mg−7.4wt.%Mn master alloys in an electric resistance furnace under the protective atmosphere of 99.0 vol.% N_2 and 1.0 vol.% SF_6. Melting was carried out at 760 °C together with mechanical stirring to obtain homogenous composition. The chemical composition of the as-cast alloy, which was analyzed by X-ray fluorescence analyzer (XRF, Magix-PW2403), is listed in Table 1. The as-cast ingot was extruded at 280 °C under a speed of 3 mm/s and an extrusion ratio of 10. The bars were used for microstructure observation, mechanical and degradation tests.

Table 1 Chemical composition of Mg−4Zn−0.2Mn−0.2Ca alloy (wt.%)

Zn	Mn	Ca	Si	Fe	Mg
4.22	0.22	0.21	<0.03	<0.01	Bal.

2.2 Microstructure and mechanical test

Analyses of phase and corrosion products were performed by X-ray diffraction (XRD, D/MAX-3C) with Cu K_α radiation (wavelength λ=0.154 nm) in the range of 20°−80°. Microstructure observation was carried out by scanning electron microscope (SEM, HITACHI S3400N) equipped with energy dispersive spectrum (EDS) and transmission electron microscope (TEM, JEM−2100FX, JEOL), respectively. Tensile and three-point bending tests

were conducted by using DNS−20 universal machine under a constant speed of 1.0 mm/min at room temperature. All specimens for tensile test were made into the dog-bone shape with 5.0 mm in gauge diameter and 25.0 mm in gauge length. The bone-plates were made of the as-extruded Mg−4Zn−0.2Mn−0.2Ca alloy by machining, and relieved-stress annealing bone-plates at 230 °C for 20 min. Three-point bending test was conducted with bone-plates in size of 25.0 mm × 4.5 mm × 1.3 mm, to evaluate their mechanical response. After 1 N pre-load, load versus displacement values were recorded to calculate the bending strength of each sample [27]. Both tensile and three-point bending tests were performed three times.

2.3 In vitro immersion test

Immersion test was conducted in a Hanks' simulated body solution with the composition of 8.00 g/L NaCl, 0.40 g/L KCl, 0.14 g/L $CaCl_2$, 0.35 g/L $NaHCO_3$, 0.1 g/L $MgCl_2·6H_2O$, 0.06 g/L $MgSO_4·7H_2O$, 0.06 g/L KH_2PO_4 and 0.06 g/L $Na_2HPO_4·12H_2O$ [28]. The ratio of sample surface area to solution volume was set as 0.4 mL/mm^2 according to the ASTM-G31-72 standard. The volume of the test solution was maintained at 100 mL for bone-plate specimens and 160 mL for dog-bone shape specimens with one sample in each container. The Hanks' solution was renewed every 2 days and its initial pH was adjusted to 7.4 with HCl or NaOH solution. After degradation, some samples were cleaned with ethanol and dried for surface morphology observation. The corrosion products on sample surfaces were cleared away by using 200 g/L of Cr_2O_3 and 10 g/L of $AgNO_3$ solution.

The mass change in vitro degradation was characterized by the normalization mass change (W_1/W_0), in which W_0 and W_1 are the masses of sample before and after removing corrosion products, respectively. The degradation rate was calculated according to the Eq. (1) [29]:

$$R=K(W_0-W_1)/(DAT) \quad (1)$$

where R is the degradation rate (mm/a), K is a constant (8.76×10^4), A is the surface area of sample (cm^2), T is the time of immersion time (h) and D is the density of sample (g/cm^3).

3 Results

3.1 Microstructure and mechanical properties of extruded Mg−4Zn−0.2Mn−0.2Ca alloy

Figure 1 shows the microstructure and corresponding EDS as well as XRD results of the

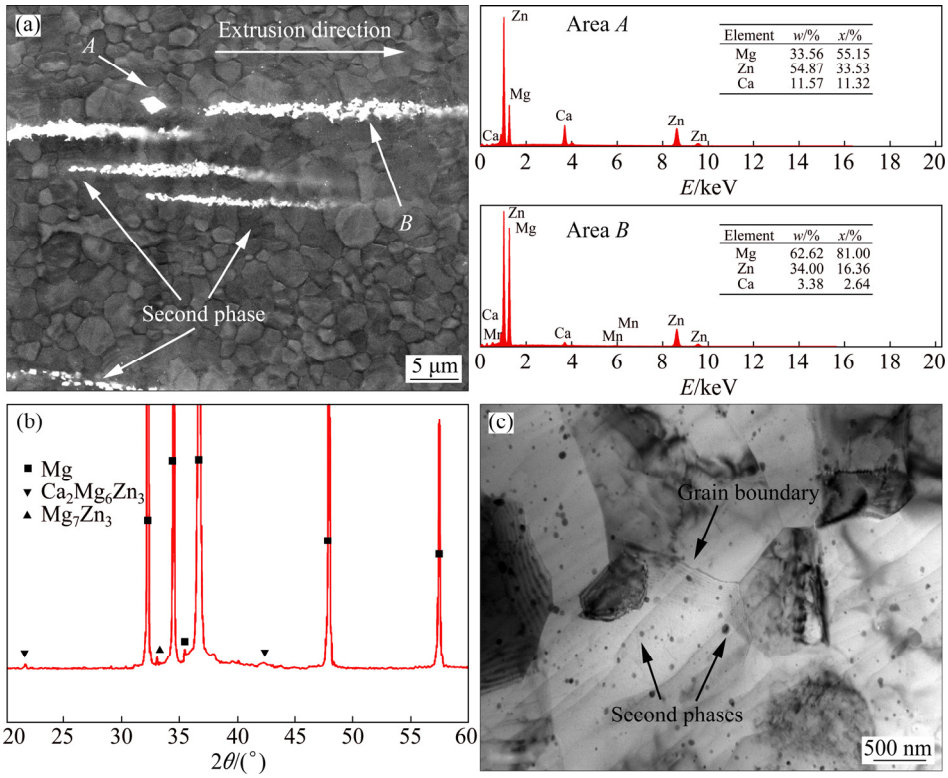

Fig. 1 Micrographs and corresponding phase analysis of as-extruded Mg−4Zn−0.2Mn−0.2Ca alloy: (a) SEM image and corresponding EDS results; (b) XRD pattern; (c) TEM image

as-extruded Mg−4Zn−0.2Mn−0.2Ca alloy. As shown in Fig. 1(a), primary second phases distribute along extrusion direction. These second phases are all composed of Mg, Zn and Ca elements. In combination of the ternary phase diagram of Mg−Ca−Zn [17] and the EDS as well as XRD results (Fig. 1(b)), the plate-shaped (Fig. 1(a), Area *A*) and the fragmented (Fig, 1(a), Area *B*) second phases are determined as Mg_7Zn_3 and $Ca_2Mg_6Zn_3$, respectively. In addition, a great number of nano granular phases are found in matrix or along grain boundaries (Fig. 1(c)).

Figure 2 shows the tensile properties of the as-extruded Mg−4Zn−0.2Mn−0.2Ca alloy as a function of immersion time in Hanks' solution. Both strength and plasticity decrease with increase in the immersion time. Particularly, the ultimate tensile strength (UTS) drops continuously during the first 90 days, whereas the yield strength (YS) declines obviously in the first and the third 30 days with a plateau appearing in the second 30 days. As listed in Table 2, the UTS, YS and elongation before immersion are 297.3 MPa, 210.1 MPa and 23.2%, respectively. Although the mechanical properties decrease as the immersion time extends, they are still 63.8 MPa, 60.3 MPa and 0.5 % after immersion for 90 days, respectively.

Figure 3 shows the cross-section morphologies of the as-extruded Mg−4Zn−0.2Mn−0.2Ca alloy after various immersion time. It is evident that the size of corrosion holes increases while the un-corroded area decreases with increase in the immersion time. As the degradation process continues, the thickness of corrosion layers increases, and the corrosion holes extend from the periphery to the center of samples.

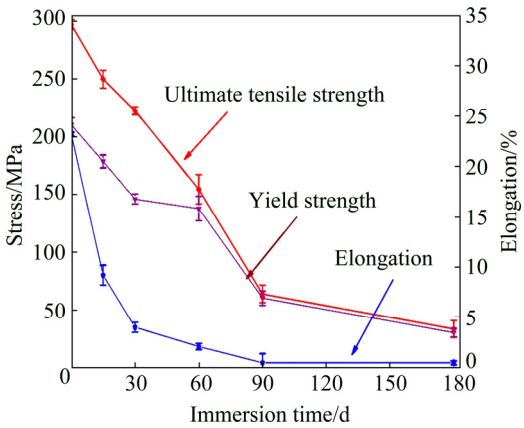

Fig. 2 Tensile properties of as-extruded alloy as function of immersion time in Hanks' solution

Table 2 Mechanical properties of as-extruded Mg−4Zn−0.2Mn−0.2Ca alloy after various immersion time in Hanks' solution

Immersion time/d	UTS/MPa	YS/MPa	Elongation/%
0	297.3±4.1	210.1±6.4	23.2±0.2
15	250.0±7.8	178.7±5.6	9.2±1.0
30	222.4±3.3	146.3±4.2	4.0±0.5
60	154.7±12.6	138.1±10.5	2.1±0.3
90	63.8±7.6	60.3±6.3	0.5±0.9
180	33.4±7.2	30.2±3.7	0.5±0.2

3.2 Degradation of bone-plates made of extruded Mg−4Zn−0.2Mn−0.2Ca alloy

Figure 4 shows the bending stress and morphology of the bone-plate after various immersion time in Hanks' solution. The detailed bending strengths of the bone-plate are listed in Table 3. It is indicated that the bending strength of the bone-plate decreases with increase in immersion time, and maintains (67.7±15.6) MPa after immersion for 60 days. In addition, the bone-plate has not fractured during the whole bending process, it is implied that the bone-plate can experience severe plastic deformation and exhibit preferable ductility.

Figure 5 shows the SEM images of the bone-plate surfaces after various immersion time in Hanks' solution. Relatively loose protective layer and a large number of corrosion particles appear on the bone-plate surface after immersion for 30 days (Figs. 5(a) and (b)). The corrosion layer gradually gets thick after immersion for 60 days (Figs. 5(c) and (d)). The thick layers appear with an accumulation of spherical particles and sheet corrosion products (Figs. 5(c) and (e)). Many micro-cracks are observed on the surface of the passivation layer, which are due to the dehydration of corrosion layers during drying process [30].

Figure 6 shows the element mapping as well as XRD pattern of the corrosion layer after immersion for 30 days. The corrosion layer includes chemical elements of Ca, P and O, and a trace of Mg element can be found at micro-cracks. The XRD result (Fig. 6(b)) confirms that the corrosion products of the bone-plate are mainly $Mg(OH)_2$ and hydroxyapatite (HA). These corrosion products are related to the reaction process between Hanks'

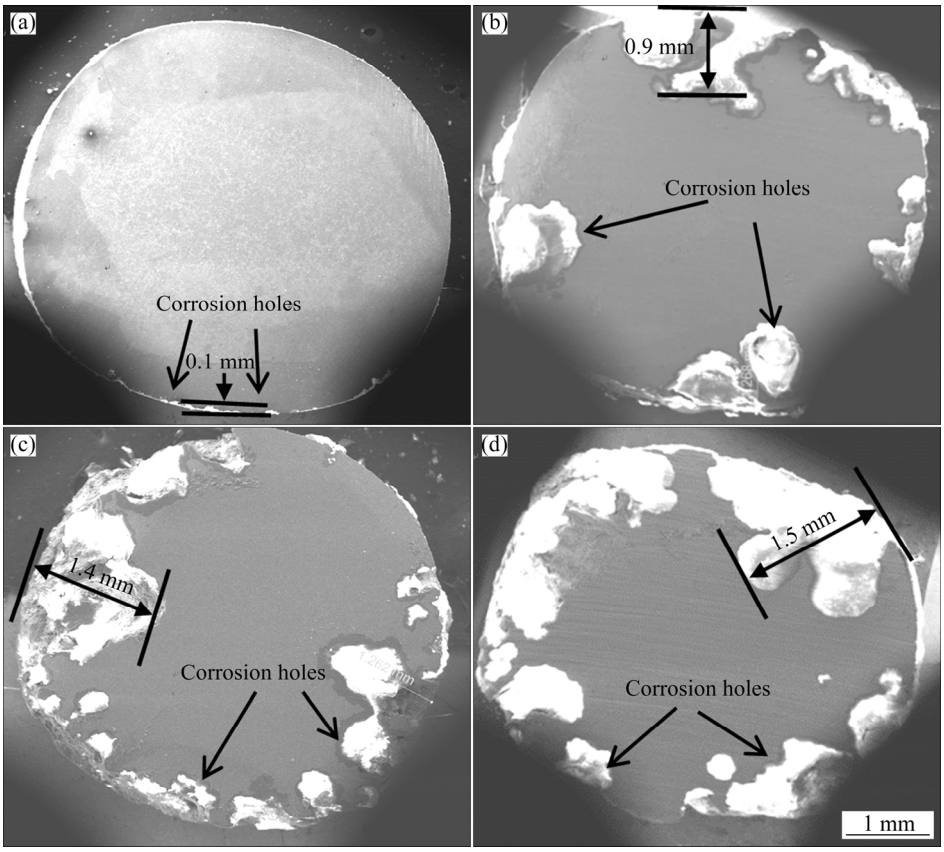

Fig. 3 Cross-section morphologies of as-extruded Mg−4Zn−0.2Mn−0.2Ca alloy after immersion for 30 days (a), 60 days (b), 90 days (c) and 180 days (d) in Hanks' solution

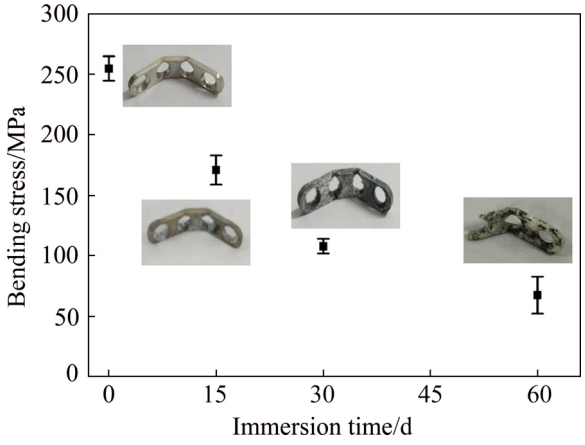

Fig. 4 Bending stress and morphology of bone-plate after various immersion time in Hanks' solution

Table 3 Bending strength of bone-plate after various immersion time in Hanks' solution

Immersion time/d	Bending strength/MPa
0	254.7±10.2
15	170.8±12.1
30	107.6±6.0
60	67.7±15.6

solution and the bone-plate, which will be discussed in Section 4.

Figure 7 shows the SEM images of the bone-plate surfaces after removing corrosion products. As shown in Fig. 7(a), a large number of small and shallow corrosion holes uniformly distribute on the surface of the bone-plate after immersion for 30 days. The size of the corrosion holes increases gradually and the adjacent small holes connect each other to form large holes as immersion process continues (Figs. 7(b) and (c)). In addition, the corrosion rate along extrusion direction is faster than that along transverse direction, indicating the corrosion of the bone-plate has directionality. From the higher magnification image (Fig. 7(d)), a large amount of corrosion pits can be found in grains as well as grain boundaries. This is mainly due to the shedding of Mg_7Zn_3 and $Ca_2Mg_6Zn_3$ phases (see Fig. 1(b)) during immersion, because they are hardly corroded in the Hanks' solution owing to their high electrode potentials [26]. The Mg matrix around these second phases is corroded preferentially during a micro-galvanic corrosion

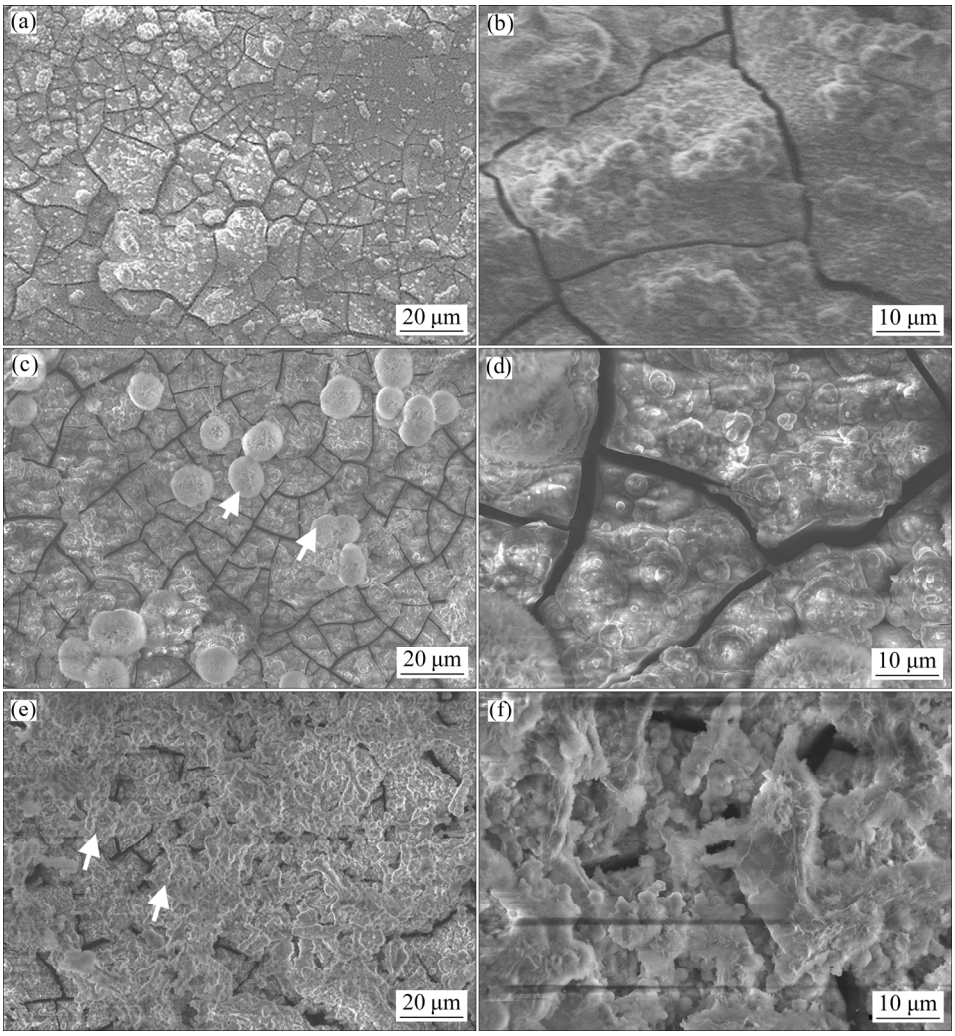

Fig. 5 SEM images of bone-plate surfaces after immersion for 30 days (a, b), 60 days (c, d) and 90 days (e, f) in Hanks' solution

process [31,32], so as to accelerate the shedding of the second phases, leading to the formation of corrosion pits.

The mass change and degradation rate of the bone-plate in vitro degradation as functions of immersion time are shown in Fig. 8. The mass continuously declines with increase in the immersion time, and about 70% of initial mass is lost after immersion for 90 days. Interestingly, the variation of degradation rate is different from the mass change. It firstly increases to the highest value on the 7th day, then decreases and reaches a gentle stage after immersion for 30−90 days. The degradation rate of the bone-plate after immersion for 90 days is only 0.84 mm/a. In fact, this variation of the degradation rate is largely attributed to the reduction in the contact area between the bone-plate and Hanks' solution.

4 Discussion

The degradation process of Mg−4Zn−0.2Mn−0.2Ca alloy can be divided into three stages. In the first stage, a prompt reaction between Mg matrix and solution occurred as

$$Mg(s)+2H_2O\rightarrow Mg(OH)_2(s)+H_2(g) \quad (2)$$

The $Mg(OH)_2$ film simultaneously formed during the reaction. This passive film separated Mg matrix from the Hanks' solution, and led to the decrease in degradation rate in the second stage, as shown in Fig. 8. However, the film was so loose that the corrosive ions (Cl^-) in Hanks' solution easily penetrated the film and reacted with the Mg matrix through Eqs. (3) and (4):

$$Mg(s)+2Cl^-(aq)\rightarrow MgCl_2 \quad (3)$$

$$Mg(OH)_2(s)+2Cl^-(aq)\rightarrow MgCl_2 \quad (4)$$

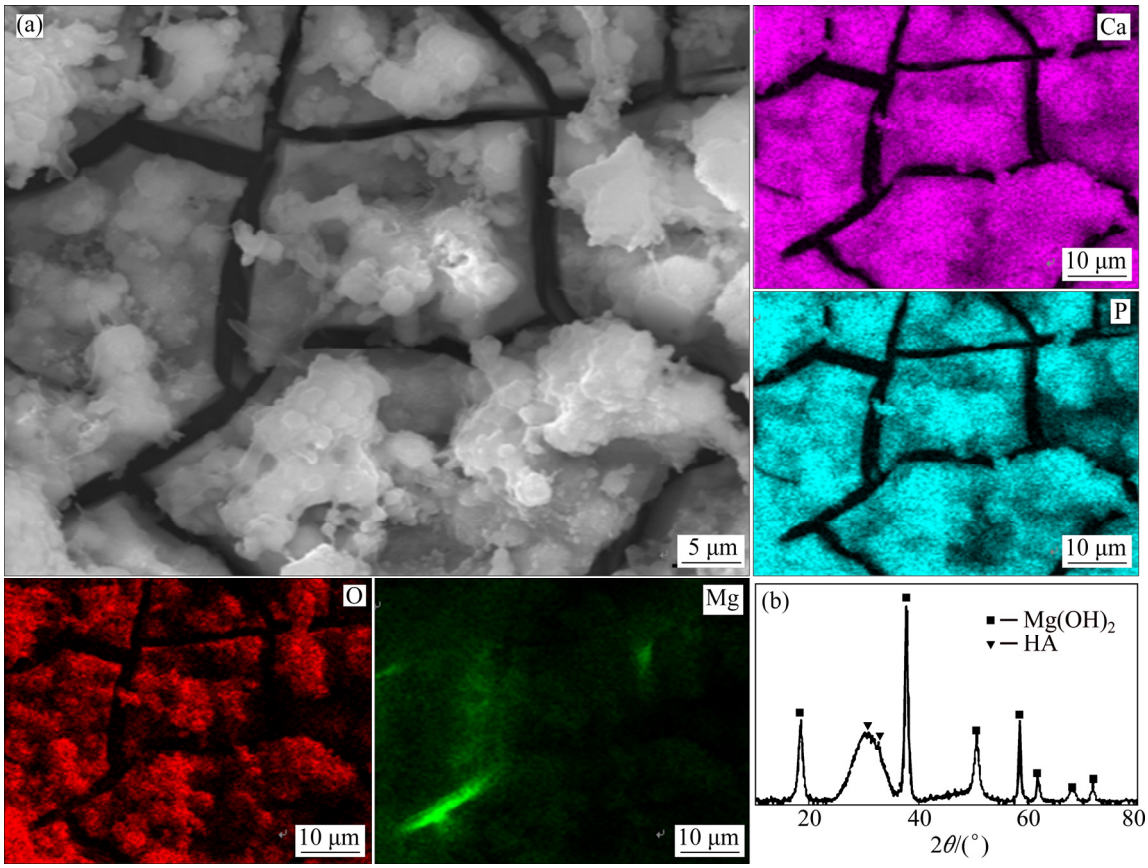

Fig. 6 SEM image and corresponding element mappings (a) and XRD pattern (b) of corrosion layer after immersion for 30 days in Hanks' solution

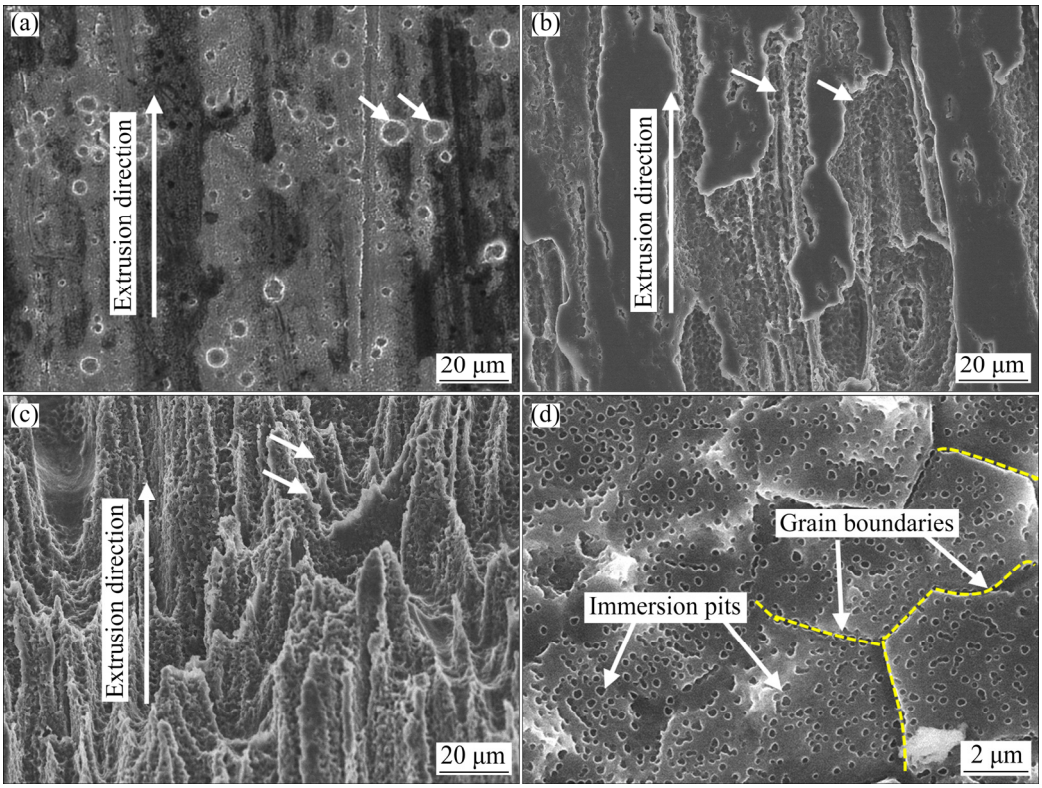

Fig. 7 SEM images of bone-plate surfaces after removing corrosion products after immersion for 30 days (a, d), 60 days (b) and 90 days (c) in Hanks' solution

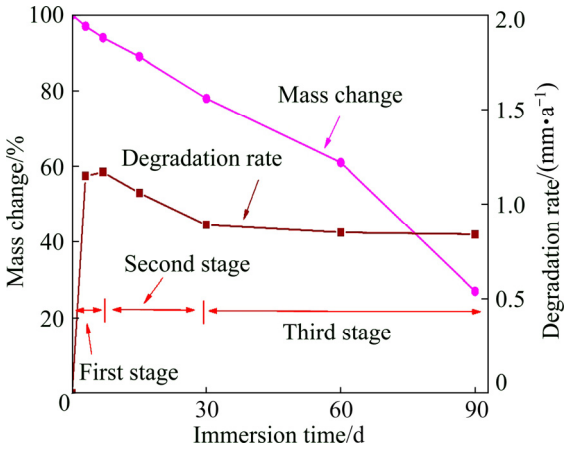

Fig. 8 Mass change and degradation rate of bone-plate in vitro degradation as function of immersion time in Hanks' solution

In addition, the integrity of the film could also be destroyed by a galvanic cell, which was made up of the second phases and the surrounding Mg matrix. With extension of the immersion time, a large amount of corrosion products deposited on the surface of the bone-plate (see Fig. 5) and separated the bone-plate from the Hanks' solution. Hence, the degradation rate was decelerated. At the same stage, the ions such as PO_4^{3-} and Ca^{2+} in Hanks' solution gathered on the surface to produce HA [$Ca_{10}(PO_4)_6(OH)_2$] (see Fig. 6(b)). The bone implants with HA usually exhibit desirable biological activity and promote growth and recovery of human bones [33,34].

The protection of $Mg(OH)_2$ film on Mg alloys is limited and this film is easy to be destroyed in the corrosive solution [35]. With the extension of corrosion time of Mg−4Zn−0.2Mn−0.2Ca alloy, the corrosion pits were firstly formed in the places which were seriously corroded (see Fig. 7(d)). The initiation of the corrosion pits was greatly associated with the second phases [36]. In this study, the Mg_7Zn_3 and $Ca_2Mg_6Zn_3$ phases acted as micro-cathodes so that the Mg matrix near these second phases was corroded preferentially. Because the second phases distributed along extrusion direction presented better continuity (Fig. 1(a)), they had an important influence on corrosion pits morphology. The separation of the continuously distributed second phases from matrix under the action of micro-galvanic couples resulted in the formation of the strip corrosion pits as shown in Fig. 7.

The corrosion spread of Mg−4Zn−0.2Mn−0.2Ca alloy is greatly associated with the corrosion pits. The corrosion rate around the corrosion pits is much higher than that at other parts of alloys once they were formed [36], because the development of the corrosion pits had an internal push "self-catalysis". Actually, due to the sharp increase of Mg^{2+} content in the corrosion pits according to reaction (2), a high cation concentration region formed and the negative ions in the solution directionally migrated to the corrosion pits to ensure the balance between positive and negative charges. The result of the above process was the accumulation of negative ions in the corrosion pits. The small radius Cl^- enrichment occurred in corrosion pits, and the corrosion product layers in the corrosion pits were severely damaged, therefore, the protective effect on the alloy matrix was remarkably reduced. The continuous expanding of the corrosion pits resulted in the formation of corrosion holes.

The corrosion holes also extended from the periphery to the center region of the sample as the immersion continued, as indicated in Fig. 3. Therefore, the protected Mg matrix area was reduced upon the formation of the corrosion holes. Furthermore, the shape of the hole-tip was irregular so that the internal curvature was inconformity in different places, which would inevitably produce a great stress concentration. As a result, the mechanical performance of the as-extruded Mg−4Zn−0.2Mn−0.2Ca alloy was aggravated owing to the corrosion holes on its surface (see Fig. 2).

5 Conclusions

(1) The ultimate tensile strength, yield strength and elongation of the Mg−4Zn−0.2Mn−0.2Ca alloy before immersion were 297.3 MPa, 210.1 MPa and 23.2%, respectively. Although the mechanical properties decreased as the immersion time extended, the values of yield strength was still 60.3 MPa after immersion for 90 days.

(2) The degradation rate of the bone-plate increased initially, but decreased gradually with immersion time, and reached 0.84 mm/a after immersion for 90 days. The bending strength of bone-plate maintained 67.7 MPa after immersion for 60 days, which indicated that the bone-plate

could bear mechanical load after long term degradation.

(3) Corrosion pits occurred in Mg matrix around the second phases under the action of micro-galvanic couples. The separation of the continuously distributed second phases from Mg matrix resulted in the formation of the strip corrosion pits and finally expanded to the corrosion holes. As a result, the mechanical performance of the Mg−4Zn−0.2Mn−0.2Ca alloy was aggravated owing to the corrosion holes on its surface.

References

[1] STAIGER M P, PIETAK A M, HUADMAI J, DIAS G. Magnesium and its alloys as orthopedic biomaterials: A review [J]. Biomaterials, 2006, 27: 1728−1734.

[2] ZENG R, DIETZEL W, WITTE F, HORT N, BLAWERT C. Progress and challenge for magnesium alloys as biomaterials [J]. Advanced Engineering Materials, 2010, 10: B3−B14.

[3] KUBASEK J, POSPÍŠILOVÁ I, VOJTĚCH D, JABLONSKA E, RUML T. Structural, mechanical and cytotoxicity characterization of as-cast biodegradable Zn−*x*Mg (*x*=0.8−8.3%) alloys [J]. Materials and Technologies, 2014, 48: 623−629.

[4] ZHANG Li-nan, HOU Zeng-tao, YE Xin, XU Zhao-bin, BAI Xue-ling, SHANG Peng. The effect of selected alloying element additions on properties of Mg-based alloy as bioimplants: A literature review [J]. Frontiers of Materials Science, 2013, 7: 227−236.

[5] CUI Lan-yue, XU Ji, LU Na, ZENG Rong-chang, ZOU Yu-hong, LI Shuo-qi, ZHANG Fen. In vitro corrosion resistance and antibacterial properties of layer-by-layer assembled chitosan/poly-L-glutamic acid coating on AZ31 magnesium alloys [J]. Transactions of Nonferrous Metals Society of China, 2017, 27: 1081−1086.

[6] LIU Ai-hui, XU Ji-lin. Preparation and corrosion resistance of superhydrophobic coatings on AZ31 magnesium alloy [J]. Transactions of Nonferrous Metals Society of China, 2018, 28: 2287−2293.

[7] ZHANG Jun-yi, KANG Zhi-xin, WANG Fen. Mechanical properties and biocorrosion resistance of the Mg−Gd−Nd−Zn−Zr alloy processed by equal channel angular pressing [J]. Materials Science & Engineering C, 2016, 68: 194−197.

[8] MA Cheng-peng, PENG Ge, NIE Lu, LIU Hai-feng, GUAN Ying-chun. Laser surface modification of Mg−Gd−Ca alloy for corrosion resistance and biocompatibility enhancement [J]. Applied Surface Science, 2018, 445: 211−216.

[9] ZENGIN H, TUREN Y, AHLATCI H, SUN Y, KARAOĞLANLI A C. Influence of Sn addition on microstructure and corrosion resistance of AS21 magnesium alloy [J]. Transactions of Nonferrous Metals Society of China, 2019, 29: 1413−1423.

[10] ZHANG Er-lin, YANG Lei, XU Jian-wei, CHEN Hai-yan. Microstructure, mechanical properties and bio-corrosion properties of Mg−Si(−Ca, Zn) alloy for biomedical application [J]. Acta Biomaterialia, 2010, 6: 1756−1762.

[11] GU Xue-nan, ZHWNG Yu-feng, CHENG Yan, ZHONG Sheng-ping, XI Ting-fei. In vitro corrosion and biocompatibility of binary magnesium alloys [J]. Biomaterials, 2009, 30: 484−498.

[12] CHEN Jun-xiu, TAN Li-yi, YU Xiao-ming, ETIM I P, IBRAHIM M, YANG Ke. Mechanical properties of magnesium alloys for medical application: A review [J]. Journal of the Mechanical Behavior of Biomedical Materials, 2018, 87: 68−79.

[13] LÜTJERING G, WILLIAMS J C, GYSLER A. Microstructure and mechanical properties of titanium alloys [J]. Materials Letters, 2009, 63: 557−559.

[14] WANG Huan-xin, GUAN Shao-kang, WANG Xiang, REN Chen-xing, WANG Li-guo. In vitro degradation and mechanical integrity of Mg−Zn−Ca alloy coated with Ca-deficient hydroxyapatite by the pulse electrodeposition process [J]. Acta Biomaterialia, 2010, 6: 1743−1748.

[15] ROSALBINO F, NEGRI S D, SACCONE A, ANGELINI E, DELFINO S. Bio-corrosion characterization of Mg−Zn−X (X=Ca, Mn, Si) alloys for biomedical applications [J]. Journal of Materials Science: Materials in Medicine, 2010, 21: 1091−1098.

[16] LI Zi-jian, GU Xun-an, LOU Si-quan, ZHENG Yu-feng. The development of binary Mg−Ca alloys for use as biodegradable materials within bone [J]. Biomaterials, 2009, 29: 1329−1344.

[17] ZANDER D, ZUMDICK N A. Influence of Ca and Zn on the microstructure and corrosion of biodegradable Mg−Ca−Zn alloys [J]. Corrosion Science, 2015, 93: 222−233.

[18] XU Li-ping, ZHANG Er-lin, YIN Dong-song, ZENG Song-yan, YANG Ke. In vitro corrosion behaviour of Mg alloys in a phosphate buffered solution for bone implant application [J]. Journal of Materials Science: Materials in Medicine, 2008, 9: 1017−1025.

[19] XU Li-ping, YU Guo-ning, ZHANG Er-lin, PAN Feng, YANG Ke. In vivo corrosion behavior of Mg−Mn−Zn alloy for bone implant application [J]. Journal of Biomedical Materials Research A, 2010, 83: 703−711.

[20] HARANDI S E, BANERJEE P C, EASTON C D, RAMAN R K S. Influence of bovine serum albumin in Hanks′ solution on the corrosion and stress corrosion cracking of a magnesium alloy [J]. Materials Science & Engineering C, 2017, 80: 335−345.

[21] ERINC M, MANNENS R, WERKOVEN G T M R. Applicability of existing magnesium alloys as biomedical implant materials [J]. San Francisco: Magnesium Technology, 2009: 209−214.

[22] WITTE F, KAESE V, HAFERKAMP H, SWITZER E, MEYERLINDENBERG A, WIRTH C J. WINDHAGEN H. In vivo corrosion of four magnesium alloys and the associated bone response [J]. Biomaterials, 2005, 26: 3557−3563.

[23] BOWEN P K, DRELICH J, GOLDMAN J. A new in vitro-in vivo correlation for bioabsorbable magnesium stents from mechanical behavior [J]. Materials Science & Engineering C, 2013, 33: 5064−5070.

[24] HE Ran-gan, LIU Ruo-yu, CHEN Qiu-bing, ZHANG Hong-ju, WANG Jing-feng, GUO Sheng-feng. In vitro

degradation behavior and cytocompatibility of Mg−6Zn−Mn alloy [J]. Materials Letters, 2018, 228: 77−80.
[25] LI Hui, PENG Qiu-ming, LI Xue-jun, LI Kun, HAN Zeng-sheng, FANG Da-qing Microstructures, mechanical and cytocompatibility of degradable Mg−Zn based orthopedic biomaterials [J]. Materials & Design, 2014, 58: 43−51.
[26] DU Wen-bo, LIU Ke, MA Ke, WANG Zhao-hui, LI Shu-bo. Effects of trace Ca/Sn addition on corrosion behaviors of biodegradable Mg−4Zn−0.2Mn alloy [J]. Journal of Magnesium and Alloys, 2018, 6: 1−14.
[27] AMY C, SAYURI Y, KOSTAS V, NICOLE M, COSTELLO B J, CHOU D T, PAL S, MAITI S. In vivo study of magnesium plate and screw degradation and bone fracture healing [J]. Acta Biomaterialia, 2015, 18: 262−269.
[28] ZHANG Xiao-bo, YUAN Guang-yin, MAO Lin, NIU Jia-lin, FU Peng-huai, DING Wen-jiang. Effects of extrusion and heat treatment on the mechanical properties and biocorrosion behaviors of a Mg−Nd−Zn−Zr alloy [J]. Journal of the Mechanical Behavior of Biomedical Materials, 2012, 7: 77−86.
[29] ASTM Standards No. G30−1972. Standard practice for laboratory immersion corrosion testing of metals1 [S]. 2004.
[30] ZHOU Wan-qiu, SHAN Da-yong, HAN En-hou, KE Wei. Structure and formation mechanism of phosphate conversion coating on die-cast AZ91D magnesium alloy [J]. Corrosion Science, 2008, 50: 329−337.
[31] ALVAREZ R B, MARTIN H J, HORSTEMEYER M F, CHANDLER M Q, WILLIAMS N, WANG P T, RUIZ A. Corrosion relationships as a function of time and surface roughness on a structural AE44 magnesium alloy [J]. Corrosion Science, 2010, 52: 1635−1648.
[32] NEIL W C, FORSYTH M, HOWLETT P C, HUTCHINSON C R, HINTON B R W. Corrosion of magnesium alloy ZE41—The role of microstructural features [J]. Corrosion Science, 2009, 51: 387−394.
[33] JAISWAL S, KUMAR R M, GUPTA P, KUMARASWAMY M, ROY P, LAHIRI D. Mechanical, corrosion and biocompatibility behaviour of Mg−3Zn−HA biodegradable composites for orthopaedic fixture accessories [J]. Journal of the Mechanical Behavior of Biomedical Materials, 2017, 78: 442−454.
[34] ABOUDZADEH N, DEHGHANIAN C, SHOKRGOZAR M A. In vitro degradation and cytotoxicity of Mg−5Zn−0.3Ca/*n*HA biocomposites prepared by powder metallurgy [J]. Transactions of Nonferrous Metals Society of China, 2018, 28: 1745−1754.
[35] HARA N, KOBAYASHI Y, KAGAYA D, AKAO N. Formation and breakdown of surface films on magnesium and its alloys in aqueous solutions [J]. Corrosion Science, 2007, 49: 166−175.
[36] SONG Ying-wei, SHAN Da-yong, HAN En-hou. Pitting corrosion of a rare earth Mg alloy GW93 [J]. Journal of Materials Science & Technology, 2017, 9: 50−56.

Mg−4Zn−0.2Mn−0.2Ca 合金经过长期体外降解后的力学性能和腐蚀行为

程元芬，杜文博，刘 轲，付军健，王朝辉，李淑波，付金龙

北京工业大学 材料科学与工程学院，北京 100124

摘 要：基于 Mg−4Zn−0.2Mn−0.2Ca 合金优良的生物兼容性，利用此挤压态合金开发可降解骨板材料。利用 Hank's 模拟溶液长期体外浸泡以及弯曲试验对骨板材料的降解性能以及力学性能进行评估。试验结果表明，该骨板降解速率在浸泡第 7 天时达到最高值，然后随着浸泡时间的延长而降低，浸泡 90 天后达到稳定(约 0.84 mm/a)。同时，经过 60 天的浸泡，其抗弯强度仍保持在 67.6 MPa，说明骨板在长期降解后仍能承受力学载荷。在微电偶作用下，连续分布的第二相与基体分离，形成点蚀坑，最终在表面腐蚀坑的作用下，合金力学性能降低。

关键词：镁合金；抗弯强度；腐蚀行为；体外降解；骨板

(Edited by Xiang-qun LI)